Some Interesting SAR Change Detection Studies

Leslie M. Novak
Scientific Systems Company, Inc.
500 West Cummings Park, Suite 3000
Woburn, MA 01801 USA

E-mail lnovak@ssci.com, novakl@charter.net

ABSTRACT

Performance results of coherent change detection (CCD) and non-coherent change detection (NCD) algorithms are presented using high-resolution synthetic aperture radar (SAR) imagery gathered by the General Dynamics Data Collection System. CCD performance comparisons using phase-only imagery versus complex (amplitude and phase) imagery are also presented. A new image quality metric, the "Universal Image Quality Index" is described and used to detect changes between a SAR intensity (reference versus test) image-pair; the change image is demonstrated to be quite similar, visually, to the corresponding CCD image – and the difference image is shown to be quite small in magnitude..

1 INTRODUCTION

Fig. 1 shows a typical SAR image gathered by the General Dynamics Data Collection System (DCS). The image size is 4096x4096 pixels and the resolution of the data is 1ft by 1ft. The red box superimposed on the image shows a region of interest containing two interesting change detection scenes that will be investigated. Non-coherent change detection studies focus on a scene containing parked vehicles (the "vehicle scene"); coherent change detection studies focus on a scene containing subtle man-made disturbances due to people walking in a grassy area (the "racetrack scene"). Figures 2 and 3 show the 1024x1024 region of interest containing the change detection scenes; Fig. 2 is the SAR reference image and Fig. 3 is the corresponding SAR test image.

FIGURE 1: SAR REFERENCE IMAGE, SIZE = 4096 x 4096 PIXELS;
AREA OF INTEREST, SIZE = 1024 x 1024 PIXELS.

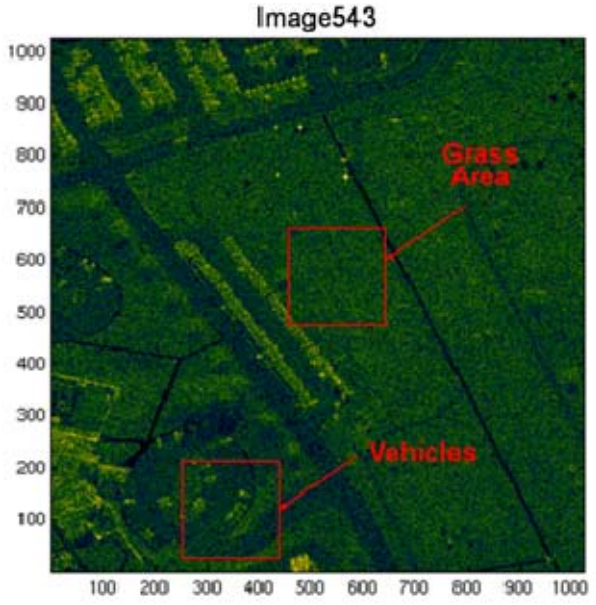

FIGURE 2: SAR REFERENCE IMAGE

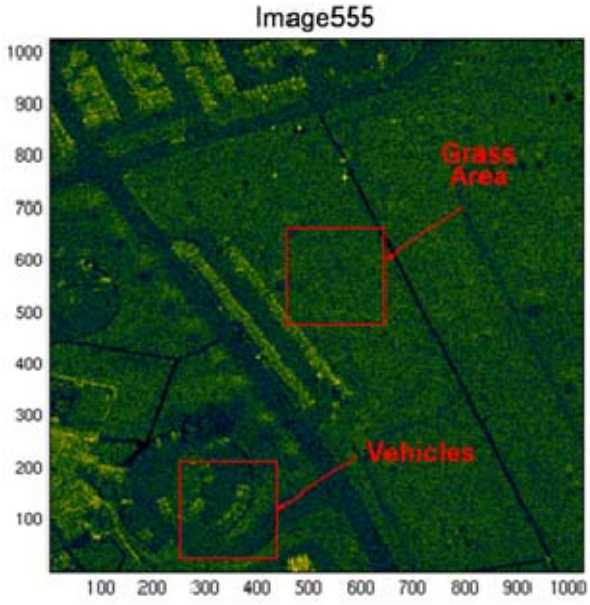

FIGURE 3: SAR TEST IMAGE

Figures 4 and 5 show the CCD and NCD change images obtained from comparisons of a test image and a previously gathered reference image; several detected changes are pointed out on the NCD and CCD images. Note that only coherent change detection has detected the “racetrack” in the grass area — and although the change in amplitude between the reference and test images is too small to be detected by the NCD algorithm, the change in phase (ie, the “coherence”) between the reference and test images is sufficient to permit detection of this subtle change by the CCD algorithm.

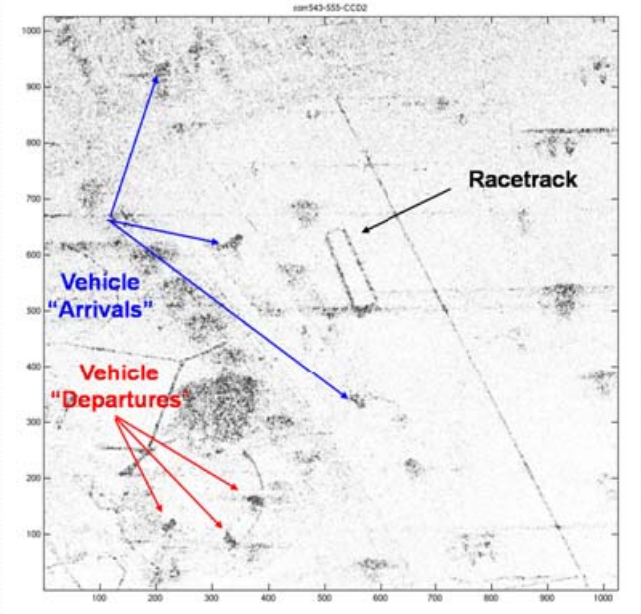

FIGURE 4: COHERENT CHANGE IMAGE

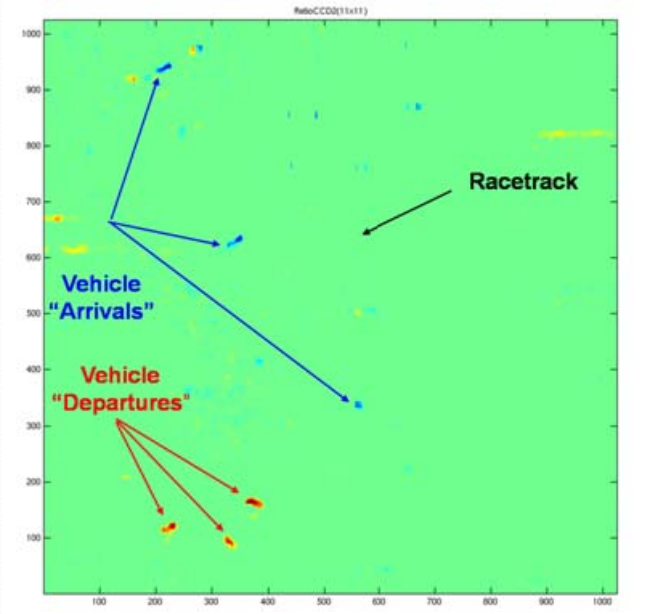

FIGURE 5: NONCOHERENT CHANGE IMAGE

2 ANALYSIS OF COHERENT CHANGE DETECTION ALGORITHM

Figure X presents a simplified block diagram of the baseline coherent change detection algorithm use in these CCD studies. The reference and test images are comprised of complex pixels, denoted as images $X_{m,n}$ and $\vec{X}_{m,n}$. As indicated in Figure 6, the algorithm calculates the coherence "γ"between the reference and test images (i.e., the magnitude of the complex cross-correlation between the reference and test images). In these studies, the coherence is calculated using a 3x3 cluster of the complex image data (thus, M = N = 2).

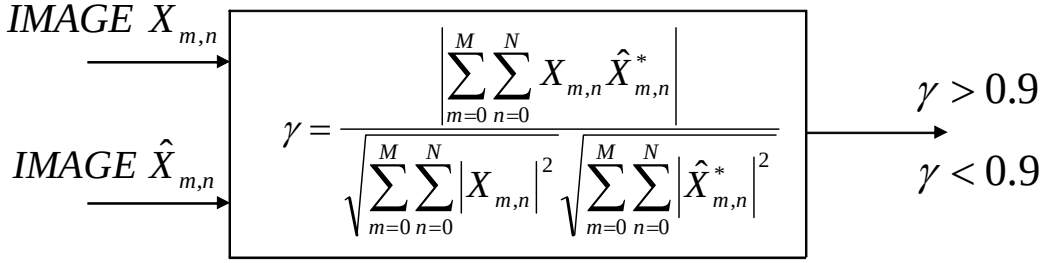

FIGURE 6: BLOCK DIAGRAM REPRESENTATION OF THE CCD ALGORITHM

Analysis of coherent change detection algorithm is given as follows. We write the complex pixel data in amplitude and phase format:

$$X_{m,n} = \left|X_{m,n}\right| e^{j\varphi_{m,n}} \quad and \quad X^{*}_{m,n} = \left|X_{m,n}\right| e^{-j\varphi_{m,n}}$$

The coherence equation defined in Figure 6, expressed in amplitude/phase format, is given as follows:

$$\gamma = \frac{\left|\sum_{m=0}^{M}\sum_{n=o}^{N}\left|X_{m,n}\right|\left|\hat{X}^{*}_{m,n}\right| e^{j(\varphi_{m,n}-\hat{\varphi}_{m,n})}\right|}{\sqrt{\sum_{m=0}^{M}\sum_{n=0}^{N}\left|X_{m,n}\right|^2}\sqrt{\sum_{m=0}^{M}\sum_{n=0}^{N}\left|\hat{X}^{*}_{m,n}\right|^2}}$$

Next we make the assumption that the magnitude of the complex reference and test pixels are equal, implying that the coherence between the images will depend only on the phase differences between pixels. With this simplifying assumption, the following result is obtained:

$$if \ \left|X_{m,n}\right| = \left|\hat{X}_{m,n}\right| = \left|X\right| \ \forall\, m,n \quad then \quad \gamma = \left|\sum_{m=0}^{M}\sum_{n=0}^{N} e^{j(\varphi_{m,n}-\hat{\varphi}_{m,n})}\right|$$

We are interested in comparing the performance of the CCD algorithm using the original complex image data versus using the phase-only data; in this study we initially focus on a sub-image of the grass area including the " racetrack feature". Figure 7 shows the 256x256 coherence sub-image containing the racetrack with a selected patch of grass outlined in red; note that the average coherence of this 256x256 sub-image is 0.9347.

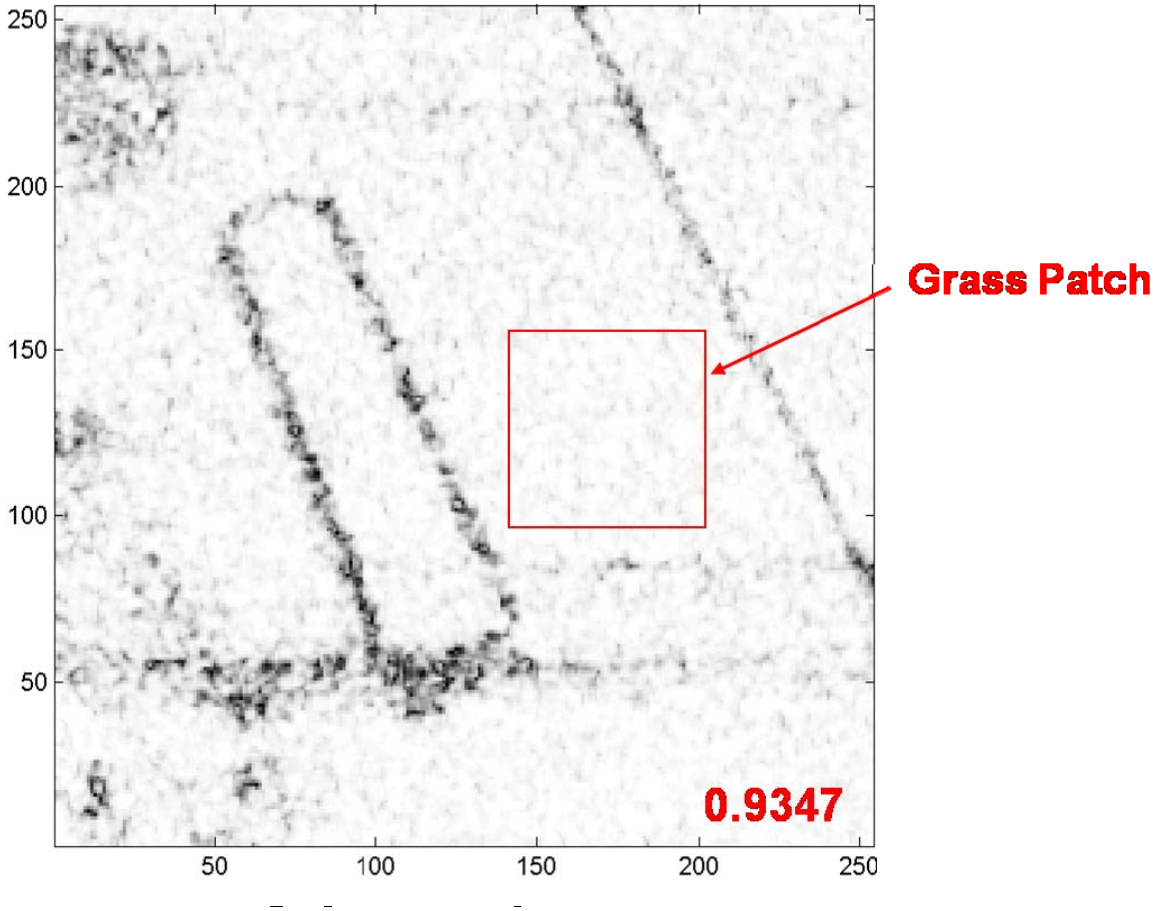

FIGURE 7: CCD IMAGE OF "RACETRACK" AREA; AVERAGE IMAGE COHERENCE = 0.9347; A GRASS PATCH IS OUTLINED

Figures 8 and 9 present a side-by-side comparison of the grass patch CCD images calculated using the original complex SAR data versus using the (amplitude-normalized) phase-only SAR data. This small patch of grass has average coherence = 0.9685 using the original complex SAR data, whereas the average coherence = 0.9361 using phase-only data. Thus, this example seems to indicate that both pixel amplitude and phase (i.e., the complex pixel) should be used in image exploitation using the CCD algorithm; there appears to be a loss in the level of coherence using phase-only images.

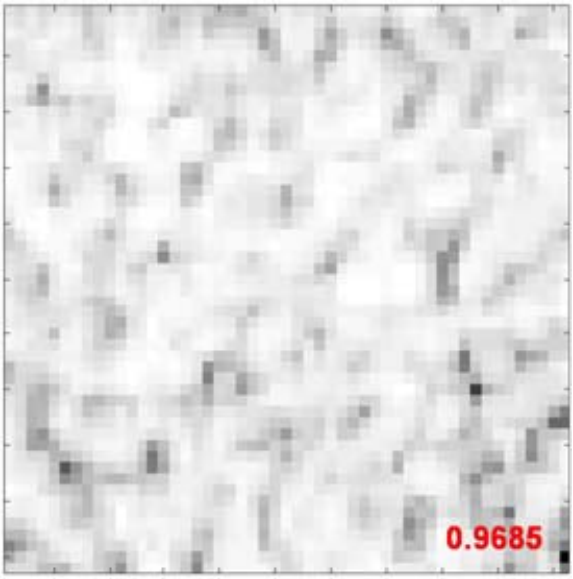

Complex Images

FIGURE 8 : SAR CCD IMAGE OF GRASS PATCH

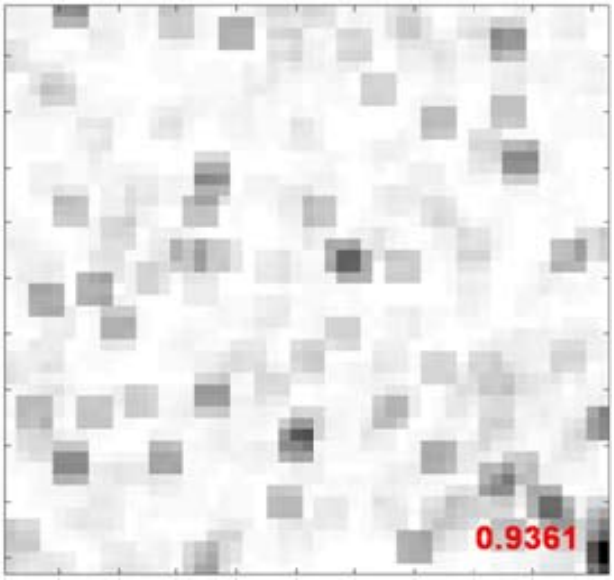

Phase-only Images

FIGURE 9: CCD IMAGE OF GRASS PATCH FROM PHASE-ONLY IMAGES

Figure 10 validates the conjecture that the best CCD image is obtained using both the amplitude and phase of the data in forming the change image; the figure indicates that the average coherence using complex data which was 0.9347 (see figure 7) has been reduced to 0.8948 using phase-only data -- and the change image in Figure 10 also shows that a larger number of low coherence pixels have been obtained using phase-only data.

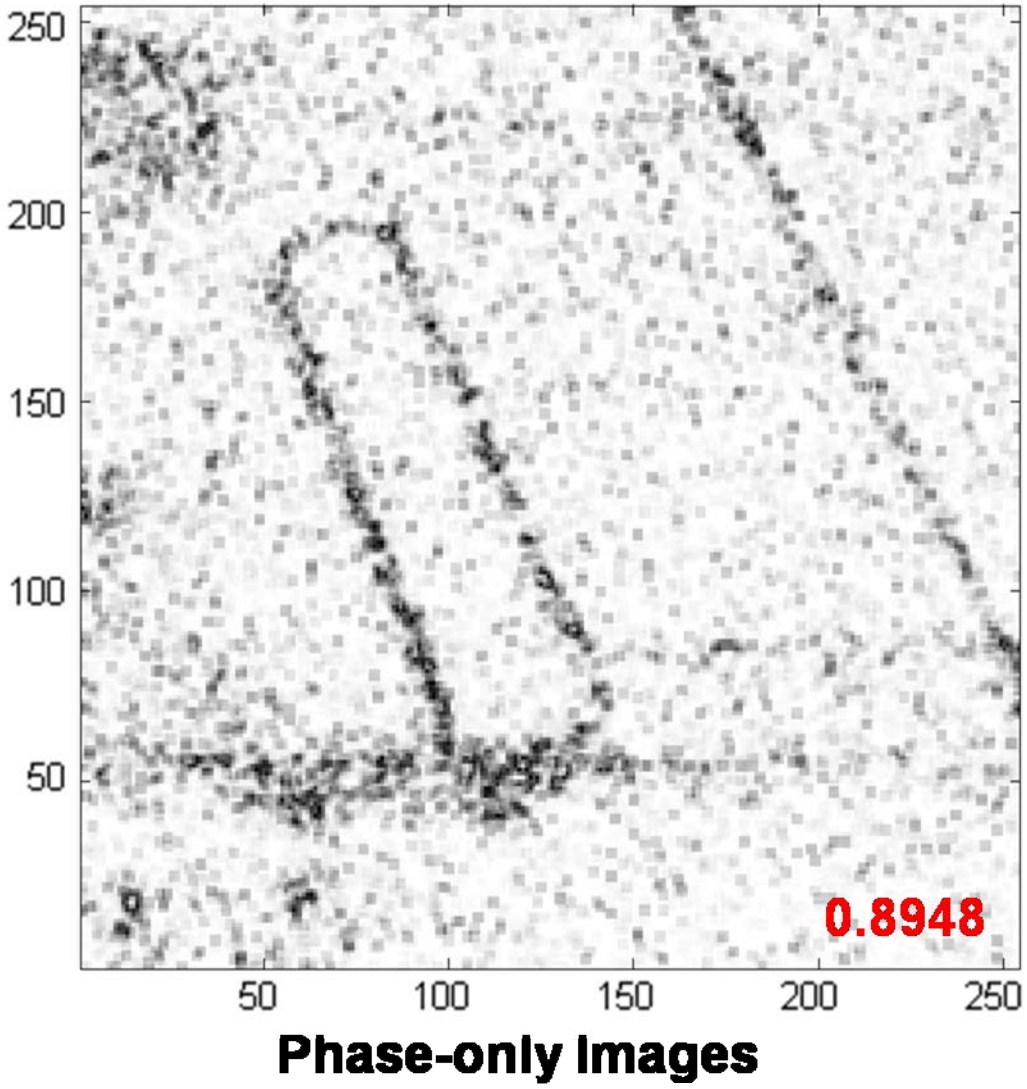

FIGURE 10: CCD IMAGE OF "RACETRACK" SCENE FROM PHASE-ONLY REFERENCE AND TEST IMAGERY

3 RESULTS USING THE "UNIVERSAL IMAGE QUALITY INDEX"

This section presents a summary of some interesting results that were obtained using an approach developed in References 5 and 6. The authors have proposed an image quality metric called the "Universal Image Quality Index" and they have demonstrated the application of their new metric to photographs such as the well-known "Lena" and others. Although our SAR images are comprised of complex pixel values, it was of interest to apply this new metric to SAR intensity images. With this goal in mind, we give a brief description of the new metric and then present results of applying the approach to the SAR imagery shown in the previously described CCD and NCD studies.

Table 1 presents details of the Universal Image Quality Index. There are two intensity images, denoted as image X and image Y; in the context of SAR change detection, X denotes the reference image (intensity image) and Y denotes the test image (intensity image). The table shows a pair of 3x3 clusters of intensity values to be compared, and our goal is to find the changes between the reference and test intensity images. The mean, variance, and covariance of the intensity values are calculated as indicated in the Table 1.

$image\ X = \begin{pmatrix} x_1 & x_2 & x_3 \\ x_4 & x_5 & x_6 \\ x_7 & x_8 & x_9 \end{pmatrix}$	$image\ Y = \begin{pmatrix} y_1 & y_2 & y_3 \\ y_4 & y_5 & y_6 \\ y_7 & y_8 & y_9 \end{pmatrix}$
$\bar{x} = \frac{1}{N}\sum_{i=1}^{N} x_i$	$\bar{y} = \frac{1}{N}\sum_{i=1}^{N} y_i$
$\sigma_x^2 = \frac{1}{(N-1)}\sum_{i=1}^{N}(x_i - \bar{x})^2$	$\sigma_y^2 = \frac{1}{(N-1)}\sum_{i=1}^{N}(y_i - \bar{y})^2$
$\sigma_{xy} = \frac{1}{(N-1)}\sum_{i=1}^{N}(x_i - \bar{x})(y_i - \bar{y})$	

TABLE 1 DEFINITION OF STATISTICS USED IN CALCULATING THE "UNIVERSAL IMAGE QUALITY INDEX"

As presented in Table 2, these mean, variance, and covariance values are used to form three image quality factors: $Q_1, Q_2, and\ Q_3$. Q_1 is a measure of structural similarity, Q_2 is a measure of the similarity of the means, and Q_3 is a measure of the similarity of the contrasts.

$$Q = \left[\frac{\sigma_{xy}}{\sigma_x \sigma_y}\right]\left[\frac{2\bar{x}\bar{y}}{(\bar{x})^2+(\bar{y})^2}\right]\left[\frac{2\sigma_x\sigma_y}{\sigma_x^2+\sigma_y^2}\right] \in [-1,+1]$$ $$Q = Q_1 \times Q_2 \times Q_3$$	
$$Q_1 = \left[\frac{\sigma_{xy}}{\sigma_x \sigma_y}\right] \in [-1,+1]$$	Q_1 : A measure of Image Structural Similarity
$$Q_2 = \left[\frac{2\bar{x}\bar{y}}{(\bar{x})^2+(\bar{y})^2}\right] \in [0,+1]$$	Q_2 : Similarity of Image means
$$Q_3 = \left[\frac{2\sigma_x\sigma_y}{\sigma_x^2+\sigma_y^2}\right] \in [0,+1]$$	Q_3 : Similarity of Image Contrasts

TABLE 2: DEFINITION OF THE "UNIVERSAL IMAGE QUALITY INDEX"

The image quality index, Q, is calculated from 3x3 clusters of intensity data at each pixel location in the image, resulting in a new image denoted as the Universal IQ Index Image; this new image is a representation of the changes that exist between the reference and test images. The SAR reference and test images shown previously in Figures 2 and 3 were converted into intensity images and processed as described above. The resulting Universal IQ Index Image we obtained is shown in Figure 11; an average IQ index of 0.8283 was obtained from the image shown. The interesting observation gleaned from the image shown in Figure 11 is that this change image visually appears to be a CCD image -- but this change image was obtained from intensity-only SAR reference and test imagery.

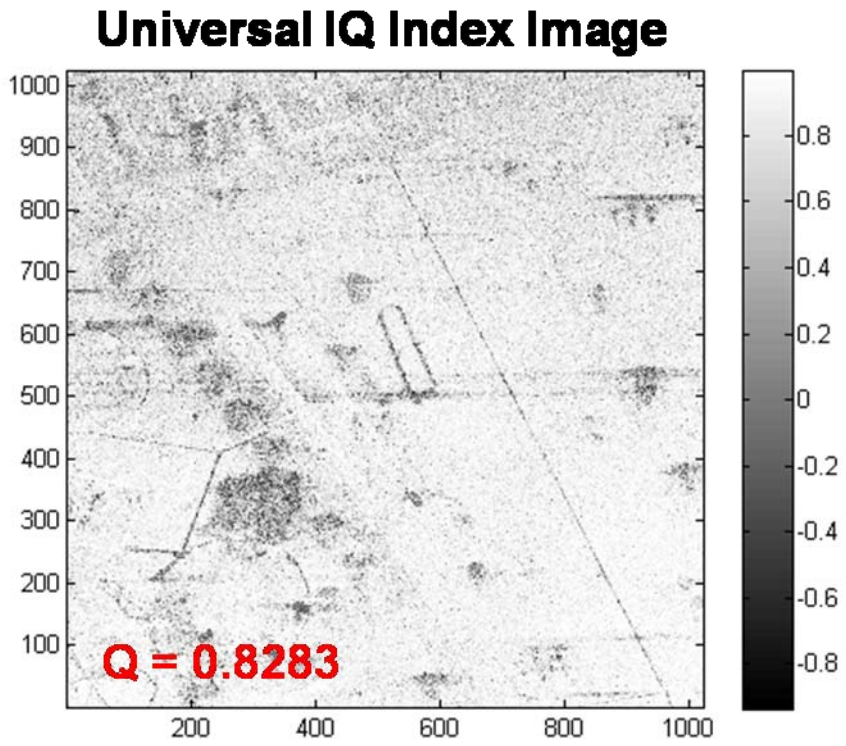

FIGURE 11: UNIVERSAL IMAGE QUALITY INDEX IMAGE OBTAINED USING INTENSITY IMAGES SHOWN IN FIGURES 2 & 3

Further analysis of the images produced by each of the factors $Q_1, Q_2, and\ Q_3$ showed that the image produced by the factor Q_1 was the dominant image, and this factor is simply the cross-correlation of the SAR intensity images. This observation has resulted in our researching the literature on previous mathematical analyses of the cross-correlation of SAR intensity images and its relationship with the SAR coherence parameter (see References 7 and 8). Table 3 presents two functional relationships derived in the references. ρ_A corresponds to intensity cross-correlation without mean removal (Reference 7) and ρ_B corresponds to intensity cross-correlation with mean removal (Reference 8).

Intensity Correlation	Coherence Relationship
ρ_A	$\gamma_A = \sqrt{2\rho_A - 1}\,; \quad \rho_A \geq 0.5$ $\gamma_A = 0\,; \quad \rho_A < 0.5$
ρ_B	$\gamma_B = \sqrt{\rho_B}\,; \quad 0 < \rho_B \leq 1.0$

TABLE 3: COHERENCE RELATIONS VS. CROSS CORRELATION OF SAR INTENSITY IMAGES

Additional SAR change detection studies using the intensity cross-correlation denoted as ρ_B in Table 3 were performed. Figure 12 presents a side-by-side comparison of the Coherence Image (left) versus the corresponding change image obtained using the intensity image cross-correlation denoted as ρ_B in Table 3. Visually these images look quite similar -- and the absolute difference between these images is presented in Figure 13. The difference error image shows reasonably small differences between the actual coherence values, γ, and the coherence estimates $\gamma_B = \sqrt{\rho_B}$.

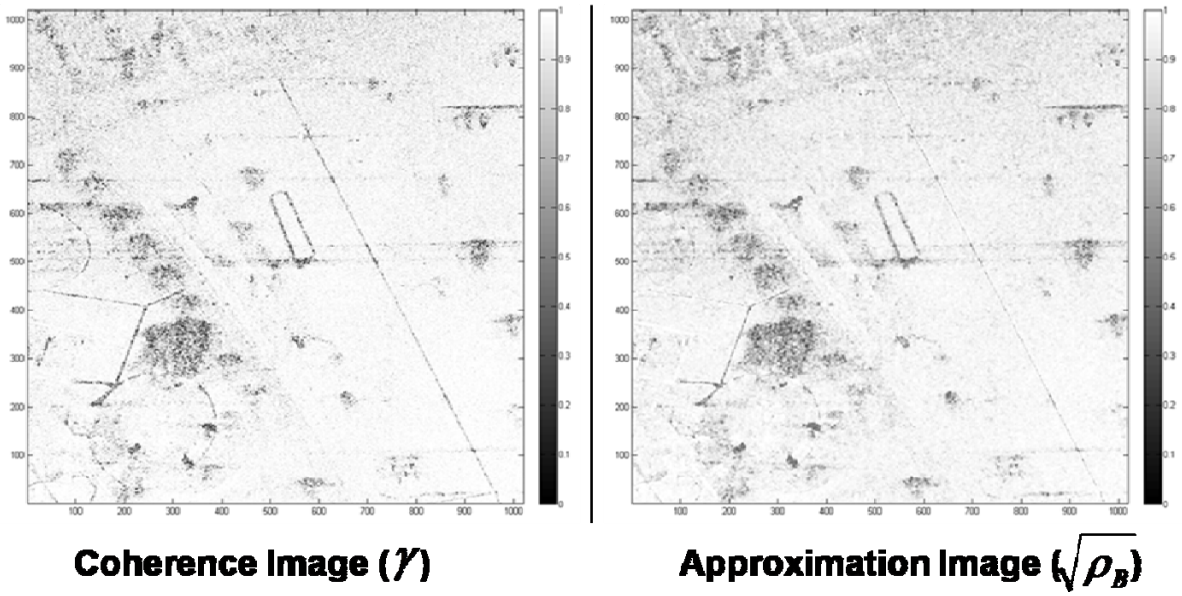

FIGURE 12: COHERENCE IMAGE VERSUS APPROXIMATION IMAGE

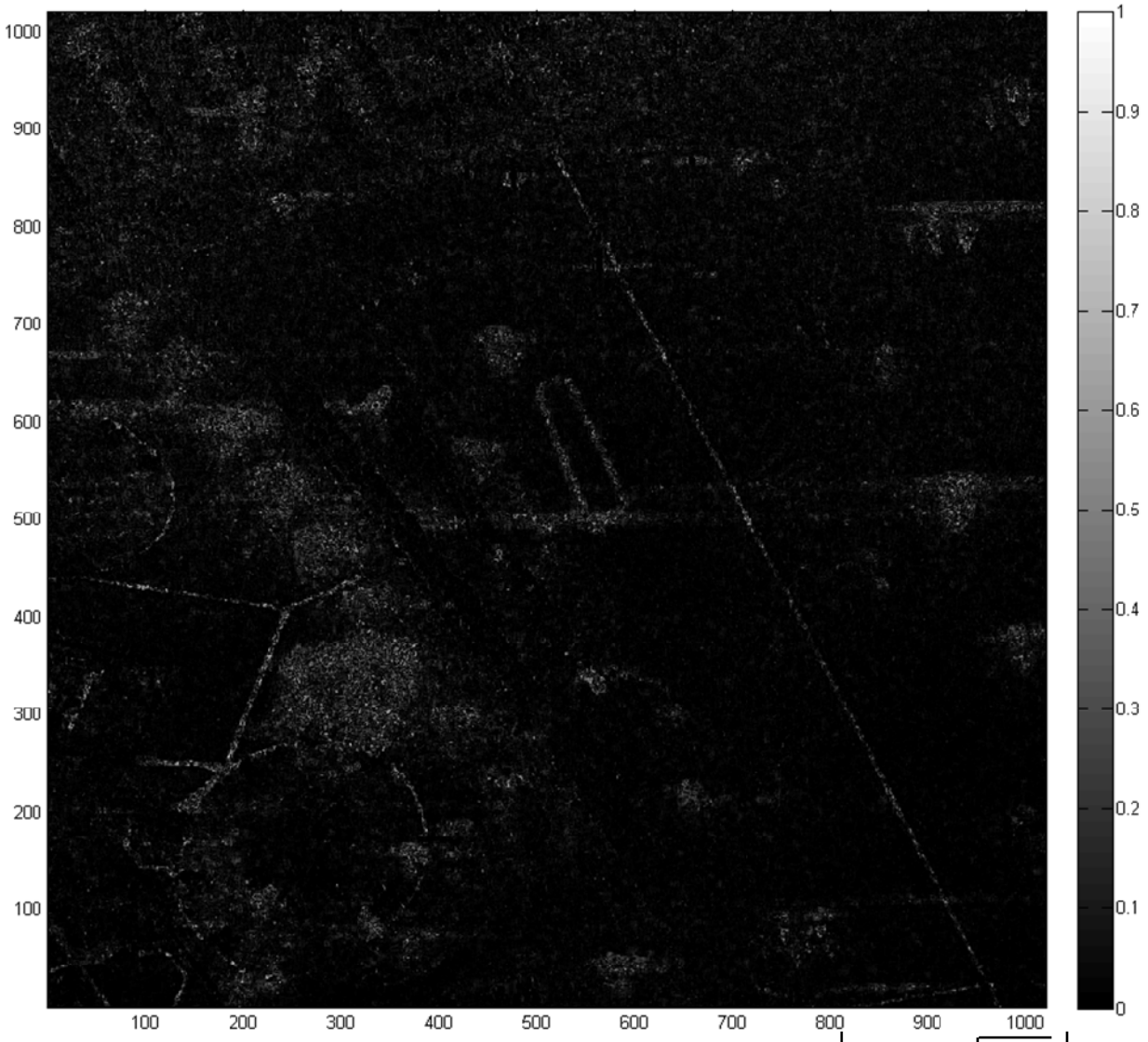

$$\left| Coherence - Approximation \right| = \left| \gamma - \sqrt{\rho_B} \right|$$

FIGURE 13: MAGNITUDE OF DIFFERENCE IMAGE

4 SUMMARY AND CONCLUSIONS

This paper reviewed some of the basic properties of SAR coherent change detection. An example was presented comparing CCD and NCD performance using a scene containing various types of changes that occurred between the SAR reference image and test image pair. Another example was presented comparing CCD performance using phase-only SAR

images versus using the complex (amplitude and phase) SAR images -- for the images used in this study we found that the coherence levels obtained from the complex imagery were somewhat better than the coherence levels obtained from the phase-only imagery.

A new image quality metric[5,6], the "Universal Image Quality Index" was investigated. Applying this image quality metric to SAR intensity images (reference versus test intensity images) we observed that the Universal IQ Image was visually quite similar to the SAR CCD coherence image. We then investigated the relationship between the coherence calculated using complex image data and the correlation calculated using the corresponding intensity images. We demonstrated that the magnitude of the differences between the actual coherence image and the estimated coherence image obtained from the correlation image were quite small, however, further analysis is needed to quantify the errors versus the registration accuracy required between reference and test images.

5 REFERENCES

[1] Novak, L. and C. Frost, "Effects of SAR Image Compression on Coherent Change Detection," SPIE Conference on Algorithms for Synthetic Aperture Radar Imagery, Orlando, FL, April, 2009
[2] Novak, L., et al, "Classifier Performance using Enhanced Resolution SAR Data," IEE Radar Conference, Edinburgh, UK, 1997
[3] Novak, L., "Change Detection for Multi-polarization, Multi-pass SAR," SPIE Conference on Algorithms for Synthetic Aperture Radar Imagery, Orlando, FL, March, 2005
[4] Novak, L., "Coherent Change Detection for Multi-polarization SAR," Asilomar Conference on Circuits, Systems, and Computers, Pacific Grove, CA, October, 2005
[5] Wang, Z. and A. Bovic, “A Universal Image Quality Index,” IEEE Signal Processing Letters, March 2002
[6] Wang, Z. and A. Bovic, “Mean Squared Error: Love It or Leave It,” IEEE Signal Processing Magazine, January 2009
[7] A. Guarnieri, C. Prati, “SAR Interferometry: A “Quick and Dirty” Coherence Estimator for Data Browsing,” IEEE Trans. G.R.S., May 1997
[8] R.Touzi, et al, “Coherence Estimation for SAR Imagery,” IEEE Trans. G.R.S., Jan.1999.